INTERNATIONAL JOURNAL FOR NUMERICAL METHODS IN FLUIDS, VOL. 24, 1049–1072 (1997)

# HIGH-ORDER SCHEMES IN BOUNDARY ELEMENT METHODS FOR TRANSIENT NON-LINEAR FREE SURFACE PROBLEMS

R. MACHANE[1] AND E. CANOT[1]*

[1]*Laboratoire des Écoulements Géophysiques et Industriels, Institut de Mecanique de Grenoble, LEGI-IMG BP 53X, F-38041, Grenoble, France*

## SUMMARY

In this paper the boundary element method is applied to solve transient non-linear free surface flow problems formulated from potential theory. For the temporal evolution a high-order time-stepping procedure based on a truncated forward-time Taylor series expansion is compared with the classical Runge–Kutta technique. The numerical code for both two-dimensional and axisymmetric configurations has been successfully implemented. Emphasis in the paper is placed on describing the analytical development achieved by the use of Maple software.
 Int. j. numer. methods fluids, 24: 1049–1072, 1997.

(No. of Figures: 13. No. of Tables: 2. No. of Refs: 22.)

KEY WORDS: free surface flow; boundary element method; Taylor series expansion; Lagrangian derivative; symbolic computation

## 1. INTRODUCTION

Free surface flows occur in a wide variety of physical phenomena: jets, drops, bubbles and cavities and gravity waves, to name just a few. All share the common feature that the domain of interest has an unknown free boundary on which a double condition has to be imposed. These types of flows are represented mathematically as non-linear initial boundary value problems. Analytical and numerical solutions have been difficult to achieve for several reasons: first, because the boundary conditions on the free surface involve quadratic functions of the velocity; second, because they are applied on a surface whose position varies with time and must be found as a part of the solutions. Analytical solutions are restricted to simple geometries and linear interface dynamics. Thus numerical solutions are necessary to treat these problems in their full generality. Furthermore, because of the non-linear terms, accurate numerical methods involving interface-tracking schemes are required to follow the free surface evolutions. Fortunately, the continuing development of high-speed digital computers has enabled us to reach these objectives. Among the various numerical techniques, the boundary element method (BEM) has proved, by its efficiency and accuracy, to be particularly well suited to problems in potential theory. The success of the integral equation formulation for treating transient non-linear problems has already been well demonstrated by Longuet-Higgins and Cokelet[1] and others. With this technique, information known on the free surface alone is used to determine its motion, thus decreasing the dimension of the problem by one. In comparison with finite element or finite

* Correspondence to: E. Canot, Laboratoire des Écoulements Géophysiques et Industriels, Institute de Mecanique de Grenoble, LEGI-IMG BP 53X, F-38041, Grenoble, France.

CCC 0271–2091/97/101049–24$17.50

*Received February 1996*
*Revised May 1996*

difference methods, the major advantage of the BEM is the avoidance of regridding of the flow region; this allows a substantial gain in computational efficiency. In other words, the development of the BEM has overcome all the difficulties encountered before with grid methods which, because of the existence of a deformable moving interface, require the time-consuming generation of a new grid over the whole computational domain at each time step. All these grid techniques are expensive and limited in their ability to resolve curved interfaces; thus they are not usually suitable for transient free boundary problems.

In the present study a numerical procedure is developed for the analysis of unsteady free interface flow problems which are formulated mathematically on the basis of potential theory. A computational model for both two-dimensional and axisymmetric flow configurations is implemented in which a high-order BEM is coupled with a high-order explicit time-stepping technique for the temporal evolution. We focus mainly on one of these aspects: the time integration part. Our main objective is the comparison of two methods of time integration: Taylor series expansions following the approach of Dold and Peregrine[2,3] and the classical Runge–Kutta method. We are especially interested in the precision of the methods, their computational efficiency, their suitability for solving transient free surface problems by the BEM and the feasibility of implementing them via a computer language. To enable this comparison, several transient hydrodynamic phenomena involving non-linear free surface effects have been studied in detail, namely gravitational flows for shallow water waves, drop oscillations and liquid jet vibrations under capillary and gravity effects.

The paper is organized as follows. In Section 2 we introduce the mathematical formulation of free surface problems in potential theory. First the boundary value problem is briefly outlined. Next, and this is the major aim of the present work, a time integration method based on Taylor series expansion is described. Then Section 3 examines the analytical development needed for the evaluation of the Taylor series terms. Section 4 is devoted to the numerical implementation of this approach. In Section 5 the performance of our computational code is illustrated by applying it to large- and small-scale test examples including two-dimensional and axisymmetric configurations. Comparison with a Runge–Kutta time integration technique is discussed in Section 6.

## 2. MATHEMATICAL FORMULATION

### *2.1. Governing equations and boundary conditions*

We consider the irrotational flow of an incompressible, inviscid fluid with a free surface. The flow can be described by a scalar potential $\varphi$, so that the velocity field $\mathbf{v}=(u, w)$ is given by

$$\mathbf{v} = \vec{\nabla}\varphi. \tag{1}$$

Thus the continuity equation in the fluid domain $\Omega(t)$ with the boundary $\Gamma(t)$ (see Figure 1) becomes a Laplace equation for $\varphi$:

$$\nabla^2\varphi = 0 \quad \text{in} \quad \Omega(t). \tag{2}$$

On the free surface $\Gamma_f(t)$ there are two boundary conditions. In the first we assume that the interface is a material surface, so that the potential $\varphi$ satisfies the kinematic boundary condition corresponding to a Lagrangian description of the free surface particles:

$$\frac{D\mathbf{r}}{Dt} = \left(\frac{\partial}{\partial t} + \mathbf{v}\cdot\vec{\nabla}\right)\mathbf{r} = \vec{\nabla}\varphi \quad \text{on} \quad \Gamma_f(t), \tag{3}$$

 

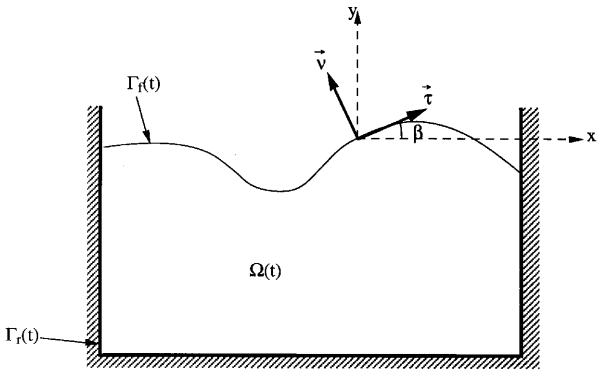


Figure 1. Definition sketch: computational domain, co-ordinates and free surface angle

where $\mathbf{r}$ defines the position vector of a free surface fluid particle and $\mathrm{D}/\mathrm{D}t$ represents the material derivative following a fluid particle. The second boundary condition on the free surface is dynamic and is derived from Bernoulli's equation combined with the normal momentum balance:

$$\frac{\mathrm{D}\varphi}{\mathrm{D}t} = \tfrac{1}{2}|\vec{\nabla}\varphi|^2 + \frac{2\sigma}{\rho}C_{\mathrm{m}} + \psi(\mathbf{r}) \quad \text{on} \quad \Gamma_{\mathrm{f}}(t), \tag{4}$$

where $\sigma$ is the surface tension, $\rho$ is the specific mass of the fluid, $C_{\mathrm{m}}$ is the average curvature of the interface and $\psi(\mathbf{r})$ defines the potential energy per unit mass associated with the body force field.

Over a rigid and impermeable boundary $\Gamma_{\mathrm{r}}(t)$ the normal velocity is continuous and is equal to zero for a fixed boundary:

$$\vec{\nabla}\varphi \cdot \vec{\nu} = \frac{\partial\varphi}{\partial n} = 0 \quad \text{on} \quad \Gamma_{\mathrm{r}}(t), \tag{5}$$

$\vec{\nu}$ being the unit outward normal vector held by the $n$- axis. This condition can of course be generalized to moving boundaries.

### *2.2. Boundary element method*

The boundary value problem described by equations (2)–(5) can be transformed, by applying Green's second identity to the velocity potential $\varphi$ (for details see e.g. References 4 and 5), into the following boundary integral equation

$$\alpha(\mathbf{r})\varphi(\mathbf{r}) = \int_{\mathbf{r}'\in\Gamma(t)} \left( \frac{\partial\varphi}{\partial n'} G(\mathbf{r},\mathbf{r}') - \varphi \frac{\partial G}{\partial n'}(\mathbf{r},\mathbf{r}') \right) \mathrm{d}\mathbf{r}', \tag{6}$$

where $G$, the Green function for equation (2), is given by

$$G(\mathbf{r},\mathbf{r}') = \frac{1}{2\pi}\log\left(\frac{1}{|\mathbf{r}-\mathbf{r}'|}\right) \quad \text{in two dimensions,} \tag{7}$$

$$G(\mathbf{r},\mathbf{r}') = \frac{1}{4\pi}\frac{1}{|\mathbf{r}-\mathbf{r}'|} \quad \text{in three dimensions,} \tag{8}$$

the coefficient $\alpha(\mathbf{r})$ is defined by

$$\alpha(\mathbf{r}) = \begin{cases} 0 & \text{if} \quad \mathbf{r} \notin \Omega(t) \cup \Gamma(t), \\ A & \text{if} \quad \mathbf{r} \in \Gamma(t), \\ 2\pi & \text{if} \quad \mathbf{r} \in \Omega(t) \text{ in two dimensions,} \\ 4\pi & \text{if} \quad \mathbf{r} \in \Omega(t) \text{ in three dimensions,} \end{cases} \tag{9}$$

 

$\mathbf{r}'$ is the integration point on the surface $\Gamma(t)$, $\mathbf{r}$ is the control point, $A$ is equal to the interior angle between the tangents $\Gamma(t)$ at point $\mathbf{r}$ and $\partial/\partial n'$ denotes the derivative in the direction of the outward normal to $\Gamma(t)$ at point $\mathbf{r}'$. For axisymmetric flow, equation (6) can be integrated in the azimuthal direction analytically to give

$$G(r,z,r',z') = \frac{-1}{4\pi}\frac{4rK(m)}{\sqrt{[(r+r')^2+(z-z')^2]}},$$
$$\frac{\partial}{\partial n'}G(r,z,r',z') = \frac{\cos\beta}{2\pi\sqrt{[(r+r')^2+(z-z')^2]}}\left[K(m)-\left(1+2r\frac{(r-r')+(z-z')\tan\beta}{(r-r')^2+(z-z')^2}\right)E(m)\right], \tag{10}$$

where $K(m)$ and $E(m)$ are complete elliptic integrals of the first and second kinds respectively[6] of modulus

$$m = \frac{4rr'}{(r+r')^2+(z-z')^2}. \tag{11}$$

First, equation (6) is written on the part of the boundary with a Neumann condition (i.e. the rigid boundary); when associated with (5), it leads to a Fredholm integral equation of the second kind. Next, equation (6) is differentiated with respect to the normal $n$ at point $\mathbf{r}$; the resultant equation is then written on the part of the boundary with a Dirichlet condition (i.e. the free surface), leading to another Fredholm integral equation of the second kind. To perform the integrations involved in these equations, the boundary is discretized into elements over which interpolation functions are applied for both the geometry and the primary variable. Within each element the geometry is defined by a couple of parametrized cubic spline interpolations and the field functions are described by cubic Hermite polynomial approximation.

In these integral equations, when the points $\mathbf{r}$ and $\mathbf{r}'$ do not coincide, the regular integrals over each segment are carried out numerically using Gaussian quadrature with the total number of required points (ranging from four to twenty-four) determined as a function of the distance between the source point and the element under consideration. However, when $\mathbf{r}$ coincides with one of the two extreme nodes defining an element, the calculation requires a separate procedure owing to the singular nature of the integrand. This last calculation is done by the technique of subtraction of the singularity: after an investigation of the asymptotic behaviour of these kernels near the singlular point, we proceed with an analytical evaluation of the integral on the singular element. For more details about the BEM see e.g. References 7 and 8.

### *2.3. Time-stepping method*

The free surface boundary conditions (3) and (4) must be integrated forward in time to establish both the new position and the potential value on the interface. Thus the following initial value problem must be solved:

$$\frac{\mathrm{D}\xi}{\mathrm{D}t} = \frac{\partial\varphi}{\partial x}, \qquad \frac{\mathrm{D}\eta}{\mathrm{D}t} = \frac{\partial\varphi}{\partial y}, \qquad \frac{\mathrm{D}\varphi}{\mathrm{D}t} = \tfrac{1}{2}|\vec{\nabla}\varphi|^2 + \frac{2\sigma}{\rho}C_{\mathrm{m}} + \psi(\xi,\eta), \tag{12}$$

where $(\xi, \eta)$ defines the co-ordinates of a fluid particle on the free surface.

 

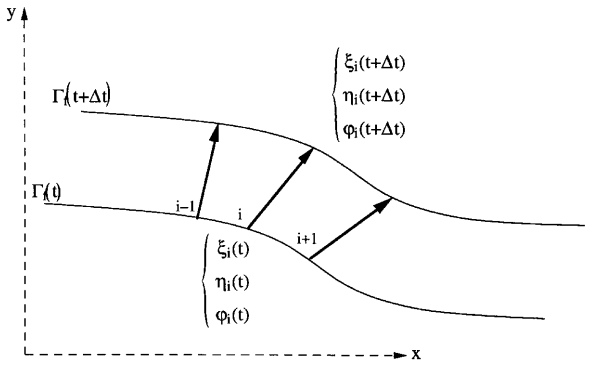


Figure 2. Movement of a fluid particle on the free surface

Following the original approach used by Dold and Peregrine,[2,3] the updating of $\Gamma_f(t)$ is based on a truncated Taylor series expansion in a Lagrangian formulation which traces the fluid particle movements on the interface (Figure 2):

$$\mathbf{r}(t+\Delta t) = \mathbf{r}(t) + \Delta t \frac{\mathrm{D}\mathbf{r}}{\mathrm{D}t} + \frac{(\Delta t)^2}{2!}\frac{\mathrm{D}^2\mathbf{r}}{\mathrm{D}t^2} + \cdots + \frac{(\Delta t)^n}{n!}\frac{\mathrm{D}^n\mathbf{r}}{\mathrm{D}t^n} + O[(\Delta t)^{n+1}], \tag{13}$$

$$\varphi(t+\Delta t) = \varphi(t) + \Delta t \frac{\mathrm{D}\varphi}{\mathrm{D}t} + \frac{(\Delta t)^2}{2!}\frac{\mathrm{D}^2\varphi}{\mathrm{D}t^2} + \cdots + \frac{(\Delta t)^n}{n!}\frac{\mathrm{D}^n\varphi}{\mathrm{D}t^n} + O[(\Delta t)^{n+1}], \tag{14}$$

where the successive Lagrangian derivates are evaluated for the same time $t$ and the fluid particles are moved with the local velocity vector. If each term of these Taylor series is evaluated, the new position of the interface and the associated velocity potential can be found. In the next section this method will be examined in detail. The analytical development needed for the evaluation of the successive terms of these Taylor series will be described.

## 3. ANALYTICAL DEVELOPMENTS

### *3.1. Differential geometry background*

We assume a fixed reference frame $(x, y)$ with the $x$-axis horizontal and the $y$-axis positive upwards. Let $(\Gamma)$ define in the $x$–$y$ plane a curve parametrized by the arc length $s$. At a given point $\mathbf{r}(s) = \mathrm{M}$ on $(\Gamma)$ we define a local Cartesian set generated by the direct orthonormal basis $(\vec{\tau}, \vec{v})$, where $\vec{\tau}$ and $\vec{v}$ are respectively the tangent and normal unit vector on $(\Gamma)$ at point M (see Figure 3). The covariant derivatives of $\vec{\tau}$ and $\vec{v}$ on $(\Gamma)$ give

$$\frac{\mathrm{d}\vec{\tau}}{\mathrm{d}s} = \kappa_1 \vec{v}, \qquad \frac{\mathrm{d}\vec{v}}{\mathrm{d}s} = -\kappa_1 \vec{\tau}, \tag{15}$$

where $\kappa_1$ defines the local curvature of $(\Gamma)$. If we define $\beta(s)$ as the inclination of the curve $(\Gamma)$ from the horizontal direction, we have evidently

$$\kappa_1 = \frac{\partial \beta}{\partial s}. \tag{16}$$

It is important to emphasize that there are two curvatures in the axisymmetric configuration. This case is examined in Appendix I.

 

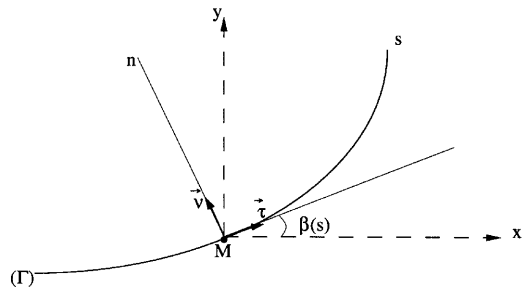


Figure 3. Definition of a local co-ordinate set on curve (Γ)

The principal advantage of this local tangent set is that it allows the evaluation of the derivatives, of any order, of any function parametrized by the arc length $s$ along (Γ). For the normal derivatives we denote by $n$ the rectilinear normal axis as a support for $\vec{\nu}$.

Furthermore, for the material derivative we can separate the advection by the local normal component of velocity from that by the tangential component:

$$\frac{\mathrm{D}.}{\mathrm{D}t} = \frac{\partial.}{\partial t} + \mathbf{v}\vec{\nabla}. = \underbrace{\frac{\partial.}{\partial t} + \frac{\partial \varphi}{\partial n}\frac{\partial.}{\partial n}}_{\Downarrow \quad \frac{\mathrm{D}_n.}{\mathrm{D}t}} + \frac{\partial \varphi}{\partial s}\frac{\partial.}{\partial s} \tag{17}$$

This form is more useful when following a moving fluid particle (with the local velocity **v**) attached to the interface. Thus we have to calculate separately the two components described above. We also point out that if the former necessitates some differential geometry tools, the latter is obtained directly from a numerical differentiation along the arc length $s$.

We get for the normal transport (for details see e.g. References 9 and 10) of the unit vectors $\vec{\tau}$ and $\vec{\nu}$

$$\frac{\mathrm{D}_n}{\mathrm{D}t}(\vec{\tau}) = \frac{\partial}{\partial s}\left(\frac{\partial \varphi}{\partial n}\right)\vec{\nu}, \qquad \frac{\mathrm{D}_n}{\mathrm{D}t}(\vec{\nu}) = -\frac{\partial}{\partial s}\left(\frac{\partial \varphi}{\partial n}\right)\vec{\tau} \tag{18}$$

and also in an equivalent way

$$\frac{\mathrm{D}_n}{\mathrm{D}t}(\beta) = \frac{\partial}{\partial s}\left(\frac{\partial \varphi}{\partial n}\right). \tag{19}$$

For the curvature terms we have

$$\frac{\mathrm{D}_n}{\mathrm{D}t}(\kappa_1) = \frac{\partial^2}{\partial s^2}\left(\frac{\partial \varphi}{\partial n}\right) + \kappa_1^2 \frac{\partial \varphi}{\partial n}, \tag{20}$$

which is obtained from (19) by using Appendix III for $\kappa_1 = \partial\beta/\partial s$.

### *3.2. Evaluation of successive terms in Taylor series*

Now our attention is focused on the evaluation of the Lagrangian time derivatives of $\xi$, $\eta$ and $\varphi$.

*3.2.1. First-order Lagrangian derivaties.* In the first stage of the computation we solve the boundary value problem

$$\nabla^2 \varphi = 0 \quad \text{in} \quad \Omega(t), \qquad \varphi = \varphi_{\mathrm{d}} \quad \text{on} \quad \Gamma_{\mathrm{f}}(t), \qquad \frac{\partial \varphi}{\partial n} = 0 \quad \text{on} \quad \Gamma_{\mathrm{r}}(t), \tag{21}$$

where the specified potential value $\varphi_{\mathrm{d}}$ is computed at the previous time step. The BEM is used to solve this Laplace problem. Note that the normal velocity component $\partial\varphi/\partial n$ on the free surface is

 

obtained from the solution of the boundary integral equation (6), but the tangential one $\partial\varphi/\partial s$ is calculated directly by numerical differentiation since the potential values are already known along the interface. Furthermore, the $x$- and $y$-components of the velocity vector are related to the tangential and normal derivatives of the potential by

$$u = \frac{\partial\varphi}{\partial x} = \frac{\partial\varphi}{\partial s}\cos\beta - \frac{\partial\varphi}{\partial n}\sin\beta, \qquad w = \frac{\partial\varphi}{\partial y} = \frac{\partial\varphi}{\partial s}\sin\beta + \frac{\partial\varphi}{\partial n}\cos\beta. \tag{22}$$

Then $\mathrm{D}\xi/\mathrm{D}t$ and $\mathrm{D}\eta/\mathrm{D}t$ are evaluated by

$$\frac{\mathrm{D}\xi}{\mathrm{D}t} = \frac{\partial\varphi}{\partial s}\cos\beta - \frac{\partial\varphi}{\partial n}\sin\beta \quad \text{on} \quad \Gamma_{\mathrm{f}}(t), \qquad \frac{\mathrm{D}\eta}{\mathrm{D}t} = \frac{\partial\varphi}{\partial s}\sin\beta + \frac{\partial\varphi}{\partial n}\cos\beta \quad \text{on} \quad \Gamma_{\mathrm{f}}(t). \tag{23}$$

$\mathrm{D}\varphi/\mathrm{D}t$ is calculated using the dynamic free surface boundary condition (4):

$$\frac{\mathrm{D}\varphi}{\mathrm{D}t} = \frac{1}{2}\left(\frac{\partial\varphi^2}{\partial s} + \frac{\partial\varphi^2}{\partial n}\right) + \frac{2\sigma}{\rho}C_{\mathrm{m}} + \psi(\xi,\eta) \quad \text{on} \quad \Gamma_{\mathrm{f}}(t). \tag{24}$$

*3.2.2. Generalization to higher-order Lagrangian derivatives.* The decomposition following (17) for a material derivative enables an evaluation of successive terms in the Taylor series expansion. The progression from order $k$ to order $k+1$ of Lagrangian derivatives is achieved in distinct stages. At first, each term in the $k$th-order Lagrangian derivative is differentiated with respect to time according to (17); to this end we use the formulations of lower-order derivatives in addition to the transport of normal and tangential derivatives as detailed in Appendices II and III. Next, direct numerical differentiation along the arc length is performed. Nevertheless, it is worthwhile to emphasize that if the first two order of Lagrangian derivatives can be evaluated easily, the evaluation of higher orders becomes intrincate and very lengthy. In fact, the number of intervening terms increases rapidly as shown later in Table I. Fortunately, the Maple software for symbolic computations can be used for any order.

For example, the second-order Lagrangian derivatives of $\xi$ and $\eta$ in a two-dimensional flow configuration[11] have analytical representations given by

$$\frac{\mathrm{D}^2\xi}{\mathrm{D}t^2} = \left[\frac{\partial\varphi_t}{\partial s} + \frac{\partial\varphi}{\partial s}\frac{\partial^2\varphi}{\partial s^2} + \frac{\partial\varphi}{\partial n}\frac{\partial}{\partial s}\left(\frac{\partial\varphi}{\partial n}\right)\right]\cos\beta + \left[-\frac{\partial\varphi_t}{\partial n} + \frac{\partial\varphi}{\partial n}\frac{\partial^2\varphi}{\partial s^2} - \frac{\partial\varphi}{\partial s}\frac{\partial}{\partial s}\left(\frac{\partial\varphi}{\partial n}\right) - \kappa_1|\vec{\nabla}\varphi|^2\right]\sin\beta, \tag{25}$$

$$\frac{\mathrm{D}^2\eta}{\mathrm{D}t^2} = \left[\frac{\partial\varphi_t}{\partial s} + \frac{\partial\varphi}{\partial s}\frac{\partial^2\varphi}{\partial s^2} + \frac{\partial\varphi}{\partial n}\frac{\partial}{\partial s}\left(\frac{\partial\varphi}{\partial n}\right)\right]\sin\beta + \left[\frac{\partial\varphi_t}{\partial n} - \frac{\partial\varphi}{\partial n}\frac{\partial^2\varphi}{\partial s^2} + \frac{\partial\varphi}{\partial s}\frac{\partial}{\partial s}\left(\frac{\partial\varphi}{\partial n}\right) + \kappa_1|\vec{\nabla}\varphi|^2\right]\cos\beta. \tag{26}$$

The corresponding terms for the axisymmetric case are outlined in Appendix I. The second-order Lagrangian derivative of $\varphi$ is evaluated with

$$\frac{\mathrm{D}^2\varphi}{\mathrm{D}t^2} = \frac{\mathrm{D}\xi}{\mathrm{D}t}\frac{\mathrm{D}^2\xi}{\mathrm{D}t^2} + \frac{\mathrm{D}\eta}{\mathrm{D}t}\frac{\mathrm{D}^2\eta}{\mathrm{D}t^2} + \frac{2\sigma}{\rho}\frac{\mathrm{D}C_{\mathrm{m}}}{\mathrm{D}t} + \frac{\mathrm{D}\psi(\xi,\eta)}{\mathrm{D}t}, \tag{27}$$

which is obtained by differentiating the dynamic boundary condition (4) with respect to time.

After the first time derivative problem (21) is solved, the Eulerian time derivative of the velocity potential, $\varphi_t = \partial\varphi/\partial t$, becomes a known quantity on the interface. However, its normal derivative $\partial\varphi_t/\partial n$ is still needed to calculate the second-order Lagrangian derivatives. By differentiating the Laplace equation (2) with respect to time, it can easily be found that $\varphi_t$ satisfies the Laplace equation

 

Table I. Summary of time integration technique using truncated Taylor series expansion (TSE). (Bernoulli equation with both capillary and gravity forces)

| TSE scheme order $k$ | Laplace problem in $\Omega(t)$ | Two-dimensional | | | Axisymmetric | | |
|---|---|---|---|---|---|---|---|
| | | Dirichlet boundary condition on $\Gamma_f(t)$ | $\frac{D^k\xi}{Dt^k}$ or $\frac{D^k\eta}{Dt^k}$ | $\frac{D^k\varphi}{Dt^k}$ | Dirichlet boundary condition on $\Gamma_f(t)$ | $\frac{D^k\xi}{Dt^k}$ or $\frac{D^k\eta}{Dt^k}$ | $\frac{D^k\varphi}{Dt^k}$ |
| 1 | $\nabla^2\varphi=0$ | $\varphi_d$: known value | 2 terms | 4 terms | $\varphi_d$: known value | 3 terms | 5 terms |
| 2 | $\nabla^2\varphi_t=0$ | $\varphi_t$: transient Bernoulli equation 4 terms | 8 terms | 10 terms | $\varphi_t$: transient Bernoulli equation 5 terms | 10 terms | 13 terms |
| 3 | $\nabla^2\varphi_{tt}=0$ | $\varphi_{tt}$: 9 terms[a] | 38 terms | 44 terms | $\varphi_{tt}$: 11 terms | 57 terms | 85 terms |
| 4 | $\nabla^2\varphi_{ttt}=0$ | $\varphi_{ttt}$: 41 terms | 143 terms | 177 terms | $\varphi_{ttt}$: 44 terms | 251 terms | 408 terms |

[a] The analytical formulation is given in Appendix IV.

too.[2,12] Thus the integral equation (6) for $\varphi$ also governs $\varphi_t$. Then we have to solve the boundary value problem

$$\nabla^2\varphi_t=0 \quad \text{in} \quad \Omega(t), \qquad \varphi_t=\frac{\mathrm{D}\varphi}{\mathrm{D}t}-\left[\left(\frac{\partial\varphi}{\partial n}\right)^2+\left(\frac{\partial\varphi}{\partial s}\right)^2\right] \quad \text{on} \quad \Gamma_f(t), \qquad \frac{\partial\varphi_t}{\partial n}=0 \quad \text{on} \quad \Gamma_r(t) \tag{28}$$

in order to obtain $\partial\varphi_t/\partial n$ on the free surface.

At third order the number of terms in the Lagrangian derivatives $\mathrm{D}^3\xi/\mathrm{D}t^3$ and $\mathrm{D}^3\eta/\mathrm{D}t^3$ is greatly increased. Moreover, the second-order Eulerian time derivative of the potential appears in these expressions. As a consequence, a new Laplace problem relative to $\varphi_{tt}=\partial^2\varphi/\partial t^2$ has to be solved. Thus, to get the coefficients of the Taylor series expansion, we solve a succession of Laplace problems for the velocity potential $\varphi$ and its Eulerian time derivatives, each solution providing the non-linear free surface boundary conditions of the next one. Indeed, the Laplace equation (2) is valid for all the time derivatives of $\varphi$.

Henceforth the time-stepping procedure following truncated Taylor series expansion will be abbreviated by TSE. In Table I the numbers of intervening terms in the Dirichlet boundary condition imposed on the interface and also in the Lagrangian derivatives of $\xi$, $\eta$ and $\varphi$ are summarized for the successive scheme orders.

## 4. NUMERICAL IMPLEMENTATION

### *4.1. Time integration procedure*

In time-dependent non-linear free surface problems a boundary integral problem is solved at each time step. Since most of the computation time is devoted to that boundary integral problem, an effective solution method is critical in the time-stepping procedure.

As mentioned in the previous section, the boundary value problems of $\varphi$ and its Eulerian time derivatives are solved by the boundary element method. This formulation starts from the integral equation (6) as we have seen in Section 2.2. To be solved, the boundary of the computational domain is described by a number of nodal points. On each element the boundary geometry is approximated by cubic splines and the field functions are represented by cubic Hermite polynomial approximation

 

(refer to Appendix V). Thus the integral equations are reduced to a set of linear algebraic equations with the unknown variables $\partial\Phi/\partial n$ on the free surface and $\Phi$ ($\Phi$ is either $\varphi$, $\varphi_t$ or a higher-order Eulerian time derivative of $\varphi$) on the remaining part of the boundary. This set is solved by the LU decomposition method.

Provided that we know the initial conditions at a given time, i.e. the domain $\Omega(t)$ and the solutions of the above-mentioned Laplace problems, we can update the free surface position and the velocity potential to the next time step. A first Laplace problem is defined for $\varphi$ and $\partial\varphi/\partial n$. Its solution provides the boundary conditions for a second Laplace problem for $\varphi_t$ and $\partial\varphi_t/\partial n$ and so on for all the successive derivatives. All these problems are expressed in the same domain geometry $\Omega(t)$. Thus several sets of equations have to be solved per time step. However, since they are formulated at the same time instant and for the same free surface profile, they have the same influence coefficient matrix. Therefore, once the integrals over each element are carried out and the coefficient matrix is decomposed into a lower and an upper triangular matrix, only forward and backward substitutions have to be done to obtain the individual solutions of the equations. In other words, numerical integrations only have to be performed once, making the method very efficient.

In the present case the computation time is dominated by that required to calculate the influence coefficients associated with the BEM, so that the explicit high-order Taylor series expansion, which maintains the same matrix coefficient during one complete time step, represents a substantial saving in CPU time when compared with Runge–Kutta integration. Indeed, the former requires information only at the beginning of the time step, whereas the latter requires information at several intermediate instants between $t$ and $t+\Delta t$. As a result, for every time step $\Delta t$ we have to resolve several Laplace problems in different geometries. Thus, with a Runge–Kutta scheme of order $k$, $k$ evaluations of the integral equations are required at each iteration and that can be extremely time-consuming.

Consequently, since most of the computing time in the BEM is spent on the calculation of the integral equations for a given geometry, it is important to minimize the amount of computational effort needed to get the desired accuracy. The explicit Taylor series expansion technique thus seems particularly suitable for transient free surface problems resolved by the BEM.[13,14]

### *4.2. Stability analysis*

To determine an appropriate time step size for the temporal evolution, a stability analysis with a linearized form of the free surface condition (4) has been performed. In the case of transient free surface problems solved by the BEM, we examine the theory of surface waves in an ideal liquid where there is no energy dissipation due to viscosity. We assume that the wave is induced either by surface tension or by gravity forces. We analyse situations where the wavelength is small in comparison with the depth of the liquid and the wave amplitude is small compared with the wavelength. Thus, with these assumptions, all the non-linear terms can be neglected. Since only surface waves are examined, the motion is confined to a region which is shallow in comparison with the depth of the liquid. Selecting the upward direction of the $y$-axis as positive, the liquid occupies the half-space $y<0$ and the velocities of the fluid must vanish at infinity: $\varphi\to 0$ as $y\to -\infty$. Let $\lambda$ be the wavelength, $a$ the wave amplitude and $\omega$ the frequency. The velocity potential of these waves is

$$\varphi(x,y,t)=a\cos(kx)\exp(ky)\sin(\omega t) \tag{29}$$

and the wave profile on the surface of the liquid is

$$\eta(x,t)=-\frac{ka}{\omega}\cos(kx)\cos(\omega t), \tag{30}$$

where $k$ is the wave number.

 

The hydrodynamic equation associated with these assumptions and the boundary conditions leads to the dispersion relation[15]

$$\omega^2 = \frac{8\pi^3\sigma}{\rho\lambda^3} + \frac{2\pi g}{\lambda}. \tag{31}$$

The frequency $\omega$, according to this formula, decreases as $\lambda$ increases and depends on both the gravity $g$ and the capillary constant $\sigma$. For long waves the main effect is caused by gravitation and the frequency depends chiefly on the term $g/\lambda$. In contrast, for short waves, surface tension plays the major role in the wave propagation.

In our computational implementation the smallest wavelength $\lambda$ which can be excited on the free surface is equal to the double the local grid spacing $\Delta s$. This assumption leads to the following stability criteria relating the time step $\Delta t$ to the grid mesh $\Delta s$:

$$\Delta t^2 \leqslant \chi(k) \cdot \Delta s \quad \text{in the gravity case,} \qquad \Delta t^2 \leqslant \gamma(k) \cdot \Delta s^3 \quad \text{in the capillary case,} \tag{32}$$

where $\chi(k)$ and $\gamma(k)$ are two constants that depend on the time integration scheme order $k$.

Note that these criteria have been obtained assuming that the amplitude of the excited mode at the end of the first time step is not larger than its amplitude at the beginning. The physics has led us to this assumption. A preferable way would be to formulate the stability problems in terms of matrices. In this manner we observe that our explicit schemes are never stable, except for the fourth-order Runge–Kutta scheme. However, semi- implicit schemes are stable and lead to criteria analogous to (32). This analysis will be the aim of another paper. It suffices to mention here that the comparison between TSE and RK schemes can be made for relatively short times before the development of instabilities.

### *4.3. Checks of computational accuracy*

Generally, two types of errors are introduced in the numerical solution of a problem. These errors and round-off error, which is a property of the computer, and discretization error, which is dependent upon the particular numerical method. Understanding and controlling these errors is essential in order to get a successful solution. The overall accuracy of our computations depends on the two numerical processes that we distinguished before, i.e. the solution of the Laplace problems at a given time, which requires the use of a spatial discretization, and the time integration, which requires a temporal one. Both the field equation solver and the time-stepping procedure can be checked independently. We will just mention the fact that adding a large number of terms together (refer to Table I) may lead to precision loss. Unfortunately, this rounding error is impossible to evaluate, except with the use of specific software.[16] We did not have the opportunity to do such a validation, but we reserve it for a future work.

*4.3.1. Error due to spatial discretization.* The boundary geometry of the computational domain is approximated by cubic splines and the field functions are described by Hermite polynomial approximation of third order. In this case the results of our numerical experiments indicate that the convergence with the grid size is cubic, so we define the error associated with the BEM solver as

$$\varepsilon_{\text{BEM}} = O(\Delta s^3). \tag{33}$$

The error (33) has been obtained from numerical tests on both Dirichlet and Neumann problems of either two-dimensional or axisymmetric flows for which analytical solutions for the velocity potential

 

$\tilde{\varphi}$ are available. Using the Euclidian norm, the relative error associated with the BEM solver is defined by

$$\varepsilon_{\mathrm{BEM}} = \frac{|\varphi - \tilde{\varphi}|}{|\tilde{\varphi}|}. \tag{34}$$

*4.3.2. Error due to time integration.* Since there are no analytical solutions available for most non-linear free boundary problems, the accuracy of the numerical results is examined by checking the mass and energy conservation laws of the fluid. Thus a global check of the time-stepping accuracy is provided by the following two relative errors defined for each time: the volume error $\varepsilon_{\mathrm{v}}(t)$ relative to the initial volume $V^{\mathrm{i}}$ of the domain $\Omega(t)$,

$$\varepsilon_{\mathrm{v}}(t) = \frac{|V(t) - V^{\mathrm{i}}|}{V^{\mathrm{i}}}, \tag{35}$$

and the total energy error $\varepsilon_{\mathrm{e}}(t)$ relative to the initial total energy $E^{\mathrm{i}}$,

$$\varepsilon_{\mathrm{e}}(t) = \frac{|E(t) - E^{\mathrm{i}}|}{E^{\mathrm{i}}}, \tag{36}$$

where the total energy $E$ is computed as the sum of the kinetic energy $E_{\mathrm{k}}$ and potential energy $E_{\mathrm{p}}$. For all the examples in the next section such quantities are typically conserved to within a few per cent (e.g. see Figure 10).

### *4.4. Derivation of a consistent formulation*

The overall accuracy of a numerical scheme is considered in two parts: that associated with the field equation (6) and that associated with the integration of the evolution equations (12). To get the same rate of convergence with respect to temporal and spatial discretization, the approximations for both the boundary geometry and the field functions in the BEM solver must be appropriate to the scheme order of the time integration procedure. Our procedure is performed using cubic spline interpolation along the boundary for the geometry and cubic Hermite polynomial approximation for the field functions as detailed in Appendix V.

Let $m$ be the order of error in the BEM such that $m = 2$ for linear variation ($C^0$ basis function) and $m = 3$ for cubic variation ($C^1$ basis function) and let $O(\Delta s^m)$ define the error associated with the BEM solver.

For example, in the case of a second-order TSE scheme the first differential equation used to update the interface position gives

$$\xi(t + \Delta t) = \xi(t) + \Delta t \frac{\mathrm{D}\xi}{\mathrm{D}t} + \frac{(\Delta t)^2}{2!} \frac{\mathrm{D}^2\xi}{\mathrm{D}t^2} + O[(\Delta t)^3]. \tag{37}$$

In this expression the first-order Lagrangian derivative $\mathrm{D}\xi/\mathrm{D}t$ is related to the normal and tangential velocity components by equation (23), whereas in the second-order derivative $\mathrm{D}^2\xi/\mathrm{D}t^2$ there are several more terms, among them $\partial\varphi_t/\partial n$ which results from two consecutive Laplace problems ($\nabla^2\varphi = 0$ then $\nabla^2\varphi_t = 0$) on the same geometric domain. The former induces an error $O(\Delta s^m)$ associated with the BEM solver, while the latter induces the same error multiplied by the matrix coefficient condition number, i.e. $O(\Delta s^m) \cdot CN(M)$.

 

Table II. Constraint on BEM solver combined with higher-order TSE

| Case | Second-order TSE | Fourth-order TSE |
|---|---|---|
| Gravity | BEM solver with first-order approximation is necessary: $\varepsilon_{\mathrm{BEM}} \approx O(\Delta s)$ | BEM solver with linear approximation is necessary: $\varepsilon_{\mathrm{BEM}} \approx O(\Delta s^2)$ |
| Capillary | BEM solver with cubic approximation is necessary: $\varepsilon_{\mathrm{BEM}} \approx O(\Delta s^3)$ | BEM solver with sixth-order approximation is necessary: $\varepsilon_{\mathrm{BEM}} \approx O(\Delta s^6)$ |

Thus on the right-hand side of (37) the first-order derivative prevails over the following ones. Therefore we can write in a consistent manner, to get effectively a second-order time integration method,

$$\Delta t \cdot O(\Delta s^m) \approx O(\Delta t^3). \tag{38}$$

Furthermore, a linear stability analysis (detailed previously in Section 4.2) has led to the criteria

$$\Delta s \approx (\Delta t)^2 \quad \text{in the gravity case,} \qquad (\Delta s)^3 \approx (\Delta t)^2 \quad \text{in the capillary case.}$$

Introducing these relations in (38) shows that $m$ must be equal to or greater than one in the gravity case and equal to three or more for the capillary case. This result implies that for problems involving only gravitational effects a BEM with a constant approximation will be enough for the second-order time-marching scheme, whereas a cubic one is necessary in problems with capillary effects.

The constraint on the BEM solver combined with higher-order TSE is presented in Table II, where we have summarized the deductions obtained from the same reasoning as presented immediately above. We can note from these results the high-order approximation needed for a consistent BEM coupled with a fourth-order TSE in the numerical solution of problems involving capillary effects; this is the reason why we have not examined this case in our computation.

## 5. APPLICATIONS

The numerical model outlined in the previous sections was implemented in a computer code and has been applied to a wide variety of transient free surface problems including two-dimensional and axisymmetric flows. In these test examples, depending on the application, the surface tension effects were either predominant or sufficiently weak so that they could be neglected. For each case, computed results using different techniques of time integration have been compared with one another. Precision and computing time requirement were the criteria examined. Numerical tests with several different time steps and mesh sizes have been performed.

For the test cases presented in this section, all the computations have been carried out on a HP/9000 Mod. 715 workstation equipped with 32 MB of RAM with peak performance equal to 50 Mips.

### *5.1. Axisymmetric flow configurations*

*5.1.1. Oscillations of a spherical globule in zero gravity*. In this application we present a study of slightly non-linear oscillations of spherical liquid drops in the absence of a surrounding fluid. When gravity is negligible, the drops formed in the break-up of a liquid jet undergo capillary oscillations about a spherical shape. In the present study the boundary integral method is applied to the axially symmetric motion of a liquid drop in zero gravity and in dynamically inactive surroundings such as a

 

vacuum or low-density gas. A uniform pressure distribution is assumed on the drop surface. Surface tension constitutes the only forcing term. The symmetry of the problem suggests the use of a spherical co-ordinate system ($R$, $\theta$, $\phi$) with the origin placed at the centre of the drop.

There is no large-amplitude theory of globule oscillations. For vibrations of the drop surface which are small compared with its radius, it is well known[17] that the axially symmetric form of the linearized solution is the superposition of modes of the form

$$R(\theta) = R_{\mathrm{m}} + \varepsilon_n P_n(\cos\theta)\cos(\omega_n t + \alpha_n) \tag{39}$$

for the surface shape and

$$\varphi(\theta) = -\frac{\omega_n R_{\mathrm{m}}}{n}\left(\frac{R}{R_{\mathrm{m}}}\right)^n \varepsilon_n P_n(\cos\theta)\sin(\omega_n t + \alpha_n) \tag{40}$$

for the velocity potential inside the drop, where $R_{\mathrm{m}}$ is the main radius of the globule, $\varepsilon_n$ is the amplitude of the $n$th mode and $P_n(\cos\theta)$ is the Legendre polynomial of order $n$ with $\theta$ the polar angle. The frequencies $\omega_n$ are given by

$$\omega_n^2 = \frac{n(n-1)(n+2)\sigma}{\rho R_{\mathrm{m}}^2}, \tag{41}$$

where $\sigma$ is the surface tension and $\rho$ is the density of the internal fluid. The problem has been non-dimensionalized by taking the radius $R_{\mathrm{m}}$ and the surface tension $\sigma$ as characteristic scales. We limit this test calculation to the numerical study of the second mode with the impulsive initial condition on the drop surface

$$R = R_{\mathrm{m}} = 1 \quad \text{and} \quad \varphi = \varphi_2 P_2(\cos\theta) \quad \text{at} \quad t = 0, \tag{42}$$

which can be thought of as applying an impulsive pressure at the initial time. Calculations have been done with an amplitude $\varphi_2 = 0{\cdot}2$. An estimation of the global accuracy has been made by checking the conservation of the sum of the kinetic energy, computed from the classical formula

$$E_{\mathrm{k}} = \frac{\rho}{2}\int_\Gamma \varphi \frac{\partial\varphi}{\partial n}\,\mathrm{d}\Gamma, \tag{43}$$

and the potential energy, reduced here to the surface energy

$$E_{\mathrm{p}} = \int_{\Gamma_{\mathrm{f}}} \sigma\,\mathrm{d}\Gamma. \tag{44}$$

The intersection of a meridian plane with the drop surface is described by $N$ equidistant nodes (Figure 4). For each value taken by $N$, the time step $\Delta t$ is related to the grid mesh $\Delta s$ by a relation obtained from an analysis of the linear stability of the capillary waves as described previously in Section 4.2.

*5.1.2. Droplet oscillations in a gravitational field.* In this example, surface tension effects are not taken into account and gravity is assumed to be the single driving force. The oscillations of the drop take place in a gravitational field defined as

$$\psi = -gR. \tag{45}$$

The gravitational potential energy per unit mass is

$$E_{\mathrm{p}} = \rho g \int_{\Gamma_{\mathrm{f}}} \tfrac{1}{4} R^2 \vec{v} \cdot \overrightarrow{i_{\mathrm{R}}}\,\mathrm{d}\Gamma, \tag{46}$$

 

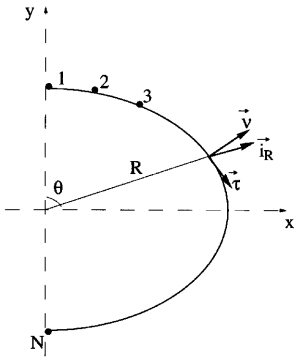


Figure 4. Axially symmetric co-ordinate system (plane $\phi = \text{const.}$)

where $\overrightarrow{i_R}$ denotes the unit vector in the radial direction. All the quantities used in the present computations are non- dimensionalized with the acceleration due to gravity and the initial radius $R_m$.

As in the first example test, the numerical study is limited to the second mode of oscillations. Figure 5 shows the drop surface profiles produced by simple oscillatory movement (of amplitude $\varphi_2 = 0{\cdot}2$) about its spherical shape.

### *5.2. Two-dimensional flow configuration*

*5.2.1. Liquid jet vibrations induced by capillary action.* This application is concerned with the oscillations of a jet of circular cross-section. An inviscid liquid emanating from a circular nozzle in a surrounding medium of negligible density forms a cylindrical jet of mean radius $R_m$. When it remains unbroken, the jet interface is subjected to an arbitrarily small vibration due to the action of capillary forces. The jet cross-section, in the case of symmetrical waves, remains circular and either contracts or expands. Let us consider the oscillations of a jet cross- section about a circular shape and limit our

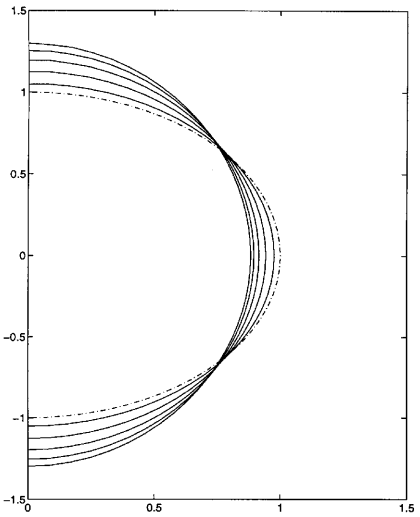


Figure 5. Profiles showing evolution of drop's shape for different time instants ($\Delta s = 0{\cdot}0785$ and $\Delta t = 0{\cdot}0638$): $-\cdot-\cdot$, initial shape; ————, profiles at every three time steps

 

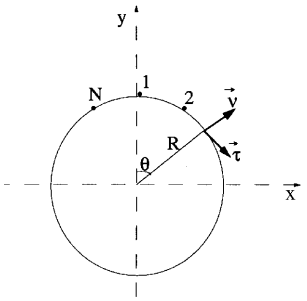


Figure 6. Discretization of jet cross-section

test to the second mode. A polar co-ordinate system ($R$, $\theta$) is fixed so that the origin lies at the centre of the cylinder. The jet cross-section is described by $N$ equidistant nodes (Figure 6). In Figure 7 the evolution of a jet cross-section is displayed for the case where the vibrations have an amplitude $\varphi_2 = 0{\cdot}4$.

*5.2.2. Propagating solitary wave.* This application is devoted to gravitational solitary wave propagation in a two-dimensional canal. The wave is initially set moving to the right as shown in Figure 8 and the surface profiles are followed in time.

The solitary wave is an approximate analytical solution in which weakly non- linear effects balance dispersive effects so that the wave maintains its original shape as it moves.[18] Figure 8 shows the computational domain for the test problem. Using the fluid depth $h$ and the velocity $\sqrt{(gh)}$ as the reference length and velocity respectively to obtain dimensionless variables, the solitary wave is generated by establishing the following initial conditions on the free surface:

$$\varphi(x, t = 0) = \frac{u_0}{k}\tanh[k(x - ct)] \quad \text{and} \quad \eta(x, t = 0) = u(c - \tfrac{1}{2}u) \quad \text{on} \quad \Gamma_f(t), \tag{47}$$

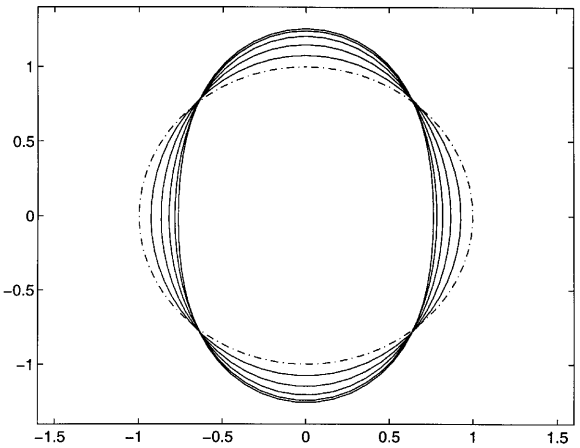


Figure 7. Successive profiles of jet cross-section for different time instants ($\Delta s = 0{\cdot}106$ and $\Delta t = 0{\cdot}0125$): −·−·−, initial shape; ————, profiles at every 10 time steps

 

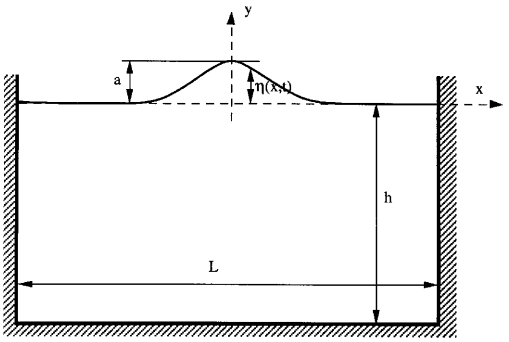


Figure 8. Flow domain for non-linear solitary wave

where the horizontal velocity field is given by

$$u(x, t) = u_0 \operatorname{sech}^2 [k(x - ct)], \tag{48}$$

with $c = \sqrt{(1 + a)}$ the wave speed, $k = \sqrt{(3a)}/2$ the wave number and $u_0 = c - \sqrt{(c^2 - 2a)}$ the velocity of the crest. The foregoing corresponds to a first-order analytical solution.

In the present flow configuration the potential energy per unit mass is reduced to the gravitational energy

$$E_p = \frac{\rho g}{2} \int_{\Gamma_f} z^2 d\Gamma. \tag{49}$$

For a computational region equal to 20 times the water depth the boundary is first discretized into cubic elements with a total of 40 nodes, of which 16 are placed on the free surface. Next, new mesh sizes are considered; each one is obtained from a reduction of the previous one by half. Figure 9 shows the computed free surface at different times as a solitary wave of amplitude $a = 0{\cdot}3$ propagates.

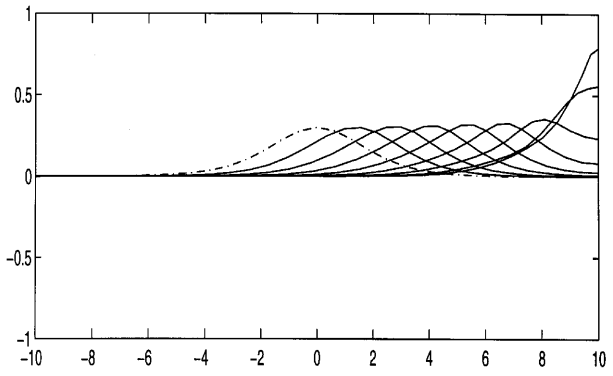


Figure 9. Free surface profiles of a solitary wave moving towards a vertical wall modelled at $x = 10$, with $\Delta s = 0{\cdot}25$ and $\Delta t = 0{\cdot}56$: – · – · , initial free surface position; ————, profiles at every two time steps

 

## 6. COMPUTATIONAL RESULTS

The results of numerical computations are illustrated in Figures 10 and 11, where time integration with truncated Taylor expansion (TSE) is compared with the Runge–Kutta (RK) technique. The purpose is to demonstrate the degree of accuracy of each approach. Indeed, our main goal is to know definitively, a precision being preselected, which time integration method is the most economic in terms of CPU time.

CPU consumption depends on several factors such as the number of numerical points employed, the duration of the run and the number of intermediate time steps. Thus at first it is worthwhile to emphasize that all the computations have been limited to short transient simulations in order to avoid the use of regridding routines.[19,20] For each application we have carried out different calculations with their respective CPU consumption and maximum error on the total energy, $\varepsilon_e$. A coarse mesh size is used first; then the grid spacing is refined progressively and in the same way the time step size is reduced. This of course causes the error $\varepsilon_e$ to decrease. We note that the value of $\varepsilon_v$, the error on the volume, is less than $10^{-4}$ in all the computations. Thus $\varepsilon_v$ is always smaller than $\varepsilon_e$.

The basic difference between TSE and RK schemes of the same order is the number of intermediate time steps. In fact, inspection of Figure 10 shows that at second order the CPU times with RK are about twice those with TSE. Indeed, this is as expected, since with the second-order RK scheme we have to solve two Laplace problems in different geometries. However, because most of the computing time is devoted to calculating the BEM matrix, the RK technique is more expensive than TSE for the same precision. Likewise comparing the two approaches at fourth order (see Figure 11), TSE requires about only one-fourth of the computing time of RK. Nevertheless, it is important to point out that the extension of TSE to higher-order schemes is not easy. In fact, we first need to build

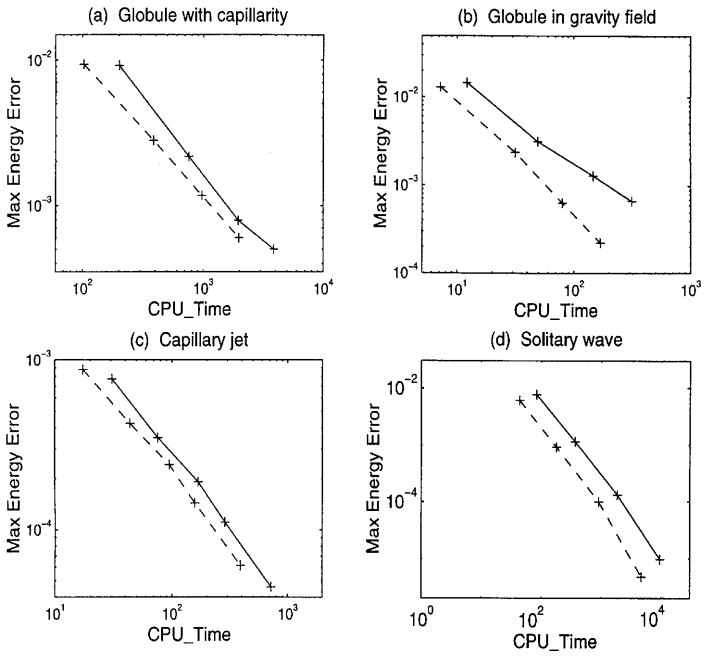


Figure 10. Comparison of precision and CPU time consumption between TSE (– – – –) and RK (————) methods of second order for different time steps. Meshing with $N$ points on the free surface: (a) $N = 20, 30, 40, 50$; (b) $N = 20, 40, 60, 80$; (c) $N = 30, 40, 50, 60, 80$; (d) $N = 16, 32, 64, 128$

 

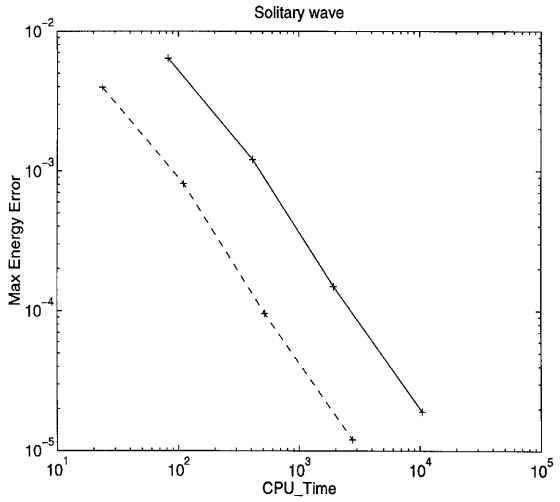


Figure 11. Comparison of precision and CPU time consumption between TSE (– – – –) and RK (————) methods of fourth order for different time steps. Meshing with $N = 16$, 32, 64, 128 points on the free surface

a procedure on Maple software to express the Lagrangian derivatives as detailed in Appendices II–IV. However, once the resulting analytical expressions are evaluated, we must translate them, using the Maple software, into Fortran language before incorporating them into our numerical code. This results in a considerable effort compared with the classical fourth-order RK technique.

## 7. CONCLUSIONS

Throughout our numerical computations it has been found that Taylor series expansion for time integration is particularly suitable for transient free surface problems solved by the BEM. This approach, developed first by Dold and Peregrine,[2,3] has been successfully used by several authors to treat non-linear water wave problems.[11,12,14] However, they have limited their studies to the gravitational case without capillary effects and restricted the computations to second-order schemes in time integration coupled with a linear approximation in the BEM solver. Since very accurate results are sometimes required, we devoted our study to the feasibility of an extension of this approach to higher orders. We have found that greater precision can be obtained using fourth-order schemes. This can be reached for the gravitational case, but the situation becomes somewhat complex when dealing with capillary waves. Furthermore, according to the capillary stability condition, an extremely high-order BEM solver would be necessary for the numerical solution of problems involving capillary effects.

## APPENDIX I: AXISYMMETRIC FLOW CONFIGURATION

For an axisymmetric flow configuration, on each point of the revolution surface, two principal curvatures are defined, namely a planar curvature $\kappa_1 = \partial\beta/\partial s$ and an axisymmetric curvature $\kappa_2 = (\sin\beta)/x$, where $x$ denotes the radial component of a cylindrical polar co-ordinate system. Thus we denote by $C_m = (\kappa_1 + \kappa_2)/2$ the local mean curvature of the interface. For convenience in writing, we will introduce the label $\kappa_3$ for the term $(\cos\beta)/x$. It is important to point out that $\kappa_3$ is not a curvature term.

 

The normal transport of these terms is formulated by

$$\frac{\mathrm{D}_n}{\mathrm{D}t}(\kappa_2) = \kappa_3 \frac{\partial}{\partial s}\left(\frac{\partial \varphi}{\partial n}\right) + \kappa_2^2 \frac{\partial \varphi}{\partial n}, \qquad \frac{\mathrm{D}_n}{\mathrm{D}t}(\kappa_3) = -\kappa_2 \frac{\partial}{\partial s}\left(\frac{\partial \varphi}{\partial n}\right) + \kappa_2 \kappa_3 \frac{\partial \varphi}{\partial n}.$$

Their derivatives along the arc length are

$$\frac{\partial \kappa_2}{\partial s} = \kappa_1 \kappa_3 - \kappa_2 \kappa_3, \qquad \frac{\partial \kappa_3}{\partial s} = -\kappa_1 \kappa_3 - \kappa_3^2.$$

In this case the second-order Lagrangian derivatives for the position of a fluid particle located on the interface have analytical representations given by

$$\begin{aligned}
\frac{\mathrm{D}^2 \xi}{\mathrm{D}t^2} &= \left[\frac{\partial \varphi_t}{\partial s} + \frac{\partial \varphi}{\partial s}\frac{\partial^2 \varphi}{\partial s^2} + \frac{\partial \varphi}{\partial n}\frac{\partial}{\partial s}\left(\frac{\partial \varphi}{\partial n}\right)\right]\cos\beta + \left[-\frac{\partial \varphi_t}{\partial n} + \frac{\partial \varphi}{\partial n}\frac{\partial^2 \varphi}{\partial s^2} - \frac{\partial \varphi}{\partial s}\frac{\partial}{\partial s}\left(\frac{\partial \varphi}{\partial n}\right) - \kappa_1 |\vec{\nabla}\varphi|^2\right. \\
&\quad \left. - \kappa_2 \left(\frac{\partial \varphi}{\partial n}\right)^2 + \kappa_3 \frac{\partial \varphi}{\partial n}\frac{\partial \varphi}{\partial s}\right]\sin\beta, \\
\frac{\mathrm{D}^2 \eta}{\mathrm{D}t^2} &= \left[\frac{\partial \varphi_t}{\partial s} + \frac{\partial \varphi}{\partial s}\frac{\partial^2 \varphi}{\partial s^2} + \frac{\partial \varphi}{\partial n}\frac{\partial}{\partial s}\left(\frac{\partial \varphi}{\partial n}\right)\right]\sin\beta + \left[\frac{\partial \varphi_t}{\partial n} - \frac{\partial \varphi}{\partial n}\frac{\partial^2 \varphi}{\partial s^2} + \frac{\partial \varphi}{\partial s}\frac{\partial}{\partial s}\left(\frac{\partial \varphi}{\partial n}\right) + \kappa_1 |\vec{\nabla}\varphi|^2\right. \\
&\quad \left. + \kappa_2 \left(\frac{\partial \varphi}{\partial n}\right)^2 - \kappa_3 \frac{\partial \varphi}{\partial n}\frac{\partial \varphi}{\partial s}\right]\cos\beta,
\end{aligned}$$

which are slightly more complicated than those corresponding to the two-dimensional configuration.

## APPENDIX II: TRANSPORT OF A NORMAL DERIVATIVE FOLLOWING NORMAL VELOCITY

Let $A$ be a scalar function dependent on time. Furthermore, $A$ is harmonic over the fluid region $\Omega(t)$. Its gradient and Eulerian time derivatives can thus be taken at each point on the interface $\Gamma_{\mathrm{f}}(t)$.

We start from

$$\frac{\partial}{\partial n}(A_t) = \vec{\nabla}\left(\frac{\partial A}{\partial t}\right)\cdot \vec{v} = \frac{\partial}{\partial t}\left(\vec{\nabla}A\right)\cdot \vec{v}.$$

However,

$$\frac{\partial}{\partial t}(\vec{\nabla}A) = \frac{\mathrm{D}_n}{\mathrm{D}t}(\vec{\nabla}A) - \frac{\partial \varphi}{\partial n}\vec{v}\cdot\vec{\nabla}(\vec{\nabla}A).$$

Then

$$\frac{\partial}{\partial t}(\vec{\nabla}A)\cdot\vec{v} = \frac{\mathrm{D}_n}{\mathrm{D}t}(\vec{\nabla}A)\cdot\vec{v} - \frac{\partial \varphi}{\partial n}\frac{\partial^2 A}{\partial n^2}.$$

The first term on the right-hand side of the last equation can be written as

$$\frac{\mathrm{D}_n}{\mathrm{D}t}(\vec{\nabla}A)\cdot\vec{v} = \frac{\mathrm{D}_n}{\mathrm{D}t}(\vec{\nabla}A\cdot\vec{v}) - \vec{\nabla}A\cdot\frac{\mathrm{D}_n\vec{v}}{\mathrm{D}t}$$

be it so

$$\frac{\mathrm{D}_n}{\mathrm{D}t}\left(\frac{\partial A}{\partial n}\right) + \frac{\partial A}{\partial s}\frac{\partial}{\partial s}\left(\frac{\partial \varphi}{\partial n}\right).$$

 

Thus we obtain

$$\frac{\partial}{\partial n}(A_t) = \frac{\mathrm{D}_n}{\mathrm{D}t}\left(\frac{\partial A}{\partial n}\right) + \frac{\partial A}{\partial s}\frac{\partial}{\partial s}\left(\frac{\partial \varphi}{\partial n}\right) - \frac{\partial \varphi}{\partial n}\frac{\partial^2 A}{\partial n^2}.$$

The general formula which enables the advection by the local normal velocity of a normal derivative $\partial A/\partial n$ of a harmonic function $A$ is therefore expressed as

$$\frac{\mathrm{D}_n}{\mathrm{D}t}\left(\frac{\partial A}{\partial n}\right) = \frac{\partial}{\partial n}(A_t) - \frac{\partial A}{\partial s}\frac{\partial}{\partial s}\left(\frac{\partial \varphi}{\partial n}\right) + \frac{\partial \varphi}{\partial n}\frac{\partial^2 A}{\partial n^2}.$$

At this stage we need to distinguish between two-dimensional and axisymmetric cases. Indeed, the Laplace equation, when expressed in the local set related to the interface, has different formulations according to the geometrical configuration. In the two-dimensional case it is written as

$$\frac{\partial^2 A}{\partial n^2} = -\frac{\partial^2 A}{\partial s^2} + \kappa_1 \frac{\partial A}{\partial n}$$

and we get the final formula

$$\frac{\mathrm{D}_n}{\mathrm{D}t}\left(\frac{\partial A}{\partial n}\right) = \frac{\partial}{\partial n}(A_t) - \frac{\partial A}{\partial s}\frac{\partial}{\partial s}\left(\frac{\partial \varphi}{\partial n}\right) - \frac{\partial \varphi}{\partial n}\frac{\partial^2 A}{\partial s^2} + \kappa_1 \frac{\partial \varphi}{\partial n}\frac{\partial A}{\partial n}. \tag{50}$$

In the axisymmetric case it gives

$$\frac{\partial^2 A}{\partial n^2} = -\frac{\partial^2 A}{\partial s^2} + (\kappa_1 + \kappa_2)\frac{\partial A}{\partial n} - \kappa_3 \frac{\partial A}{\partial s}$$

and we obtain finally

$$\frac{\mathrm{D}_n}{\mathrm{D}t}\left(\frac{\partial A}{\partial n}\right) = \frac{\partial}{\partial n}(A_t) - \frac{\partial A}{\partial s}\frac{\partial}{\partial s}\left(\frac{\partial \varphi}{\partial n}\right) - \frac{\partial \varphi}{\partial n}\frac{\partial^2 A}{\partial s^2} + (\kappa_1 + \kappa_2)\frac{\partial \varphi}{\partial n}\frac{\partial A}{\partial n} - \kappa_3 \frac{\partial \varphi}{\partial n}\frac{\partial A}{\partial s}. \tag{51}$$

## APPENDIX III: NORMAL TRANSPORT OF A COVARIANT DERIVATIVE

Let $A$ be a scalar function dependent on time, not necessarily harmonic, defined over the fluid region $\Omega(t)$. Its gradient and Eulerian time derivatives can thus be taken at each point on the interface $\Gamma_{\mathrm{f}}(t)$.

We start from

$$\frac{\partial}{\partial s}(A_t) = \vec{\nabla}\left(\frac{\partial A}{\partial t}\right) \cdot \vec{\tau} = \frac{\partial}{\partial t}(\vec{\nabla} A) \cdot \vec{\tau}.$$

However,

$$\frac{\partial}{\partial t}(\vec{\nabla} A) = \frac{\mathrm{D}_n}{\mathrm{D}t}(\vec{\nabla} A) - \frac{\partial \varphi}{\partial n}\vec{v} \cdot \vec{\nabla}(\vec{\nabla} A).$$

Then

$$\frac{\partial}{\partial t}(\vec{\nabla} A) \cdot \vec{\tau} = \frac{\mathrm{D}_n}{\mathrm{D}t}(\vec{\nabla} A) \cdot \vec{\tau} - \frac{\partial \varphi}{\partial n}[\vec{v} \cdot \vec{\nabla}(\vec{\nabla} A)] \cdot \vec{\tau}.$$

The first term on the right-hand side of the last equation can be written as

$$\frac{\mathrm{D}_n}{\mathrm{D}t}(\vec{\nabla} A) \cdot \vec{\tau} = \frac{\mathrm{D}_n}{\mathrm{D}t}(\vec{\nabla} A \cdot \vec{\tau}) - \vec{\nabla} A \cdot \frac{\mathrm{D}_n \vec{\tau}}{\mathrm{D}t}$$

 

be it so

$$\frac{\mathrm{D}_n}{\mathrm{D}t}\left(\frac{\partial A}{\partial s}\right) - \frac{\partial A}{\partial n}\frac{\partial}{\partial s}\left(\frac{\partial \varphi}{\partial n}\right).$$

Moreover,

$$[\vec{v}\cdot\vec{\nabla}(\vec{\nabla}A)]\cdot\vec{\tau} = \frac{\partial}{\partial s}\left(\frac{\partial A}{\partial n}\right) + \kappa_1\frac{\partial A}{\partial s}.$$

We obtain then

$$\frac{\partial}{\partial s}(A_t) = \frac{\mathrm{D}_n}{\mathrm{D}t}\left(\frac{\partial A}{\partial s}\right) - \frac{\partial}{\partial s}\left(\frac{\partial \varphi}{\partial n}\right)\frac{\partial A}{\partial n} - \frac{\partial \varphi}{\partial n}\frac{\partial}{\partial s}\left(\frac{\partial A}{\partial n}\right) - \kappa_1\frac{\partial \varphi}{\partial n}\frac{\partial A}{\partial s}.$$

However,

$$\frac{\partial}{\partial s}(A_t) = \frac{\partial}{\partial s}\left(\frac{\mathrm{D}_n A}{\mathrm{D}t} - \frac{\partial \varphi}{\partial n}\frac{\partial A}{\partial n}\right) = \frac{\partial}{\partial s}\left(\frac{\mathrm{D}_n A}{\mathrm{D}t}\right) - \frac{\partial}{\partial s}\left(\frac{\partial \varphi}{\partial n}\right)\frac{\partial A}{\partial n} - \frac{\partial \varphi}{\partial n}\frac{\partial}{\partial s}\left(\frac{\partial A}{\partial n}\right).$$

The general formula for the advection by the local normal velocity of a covariant derivative $\partial A/\partial s$ is thus expressed as

$$\frac{\mathrm{D}_n}{\mathrm{D}t}\left(\frac{\partial A}{\partial s}\right) = \frac{\partial}{\partial s}\left(\frac{\mathrm{D}_n A}{\mathrm{D}t}\right) + \kappa_1\frac{\partial \varphi}{\partial n}\frac{\partial A}{\partial s}. \tag{52}$$

We assume now that the function $A$ is not defined on the interface; in this case, only the component $\partial A/\partial s$ of its gradient has a meaning. Thus we introduce $\bar{A}$ as the extended function of $A$ over all space:

$$\bar{A} = A \quad \text{on the interface}, \qquad \frac{\partial \bar{A}}{\partial n} = 0 \quad \text{on the interface}, \qquad \frac{\partial \bar{A}}{\partial s} = \frac{\partial A}{\partial s} \quad \text{on the interface}.$$

We also point out that this extension is not unique, but its existence is wide enough. The previous formulae are thus applied to $\bar{A}$ and we can see that equation (52) is still valid if $A$ is defined only on the interface.

## APPENDIX IV: HIGH-ORDER DERIVATION OF DIRICHLET BOUNDARY CONDITION ON THE INTERFACE

At first order the Dirichlet boundary condition imposed on the interface $\Gamma_{\mathrm{f}}(t)$ corresponds to

$$\varphi = \varphi_{\mathrm{d}},$$

where the specified potential value $\varphi_{\mathrm{d}}$ is either computed at the previous time step or given by the initial conditions.

At second order, furthermore, we have to resolve a Laplace problem relative to $\varphi_t$. For this purpose the transient Bernoulli equation applied on the interface provides directly the boundary condition

$$\varphi_t = -\tfrac{1}{2}|\vec{\nabla}\varphi|^2 + \frac{2\sigma}{\rho}C_{\mathrm{m}} + \psi(\xi,\eta) \quad \text{on} \quad \Gamma_{\mathrm{f}}(t).$$

 

At higher order the analysis becomes slightly more complicated. Nevertheless, we can quickly achieve our objective owing the Maple software. Thus, to express the Dirichlet boundary condition at order $k+1$, we apply the following rule which makes use of a recursive calculation:

$$\varphi^{k+1} = \frac{\partial}{\partial t}(\varphi^{(k)}) = \underbrace{\frac{\mathrm{D}_n}{\mathrm{D}t}(\varphi^{(k)})}_{\Downarrow} - \frac{\partial \varphi}{\partial n}\underbrace{\frac{\partial \varphi^{(k)}}{\partial n}}_{\Downarrow},$$

recursive calculus — solution of $\nabla^2 \varphi^{(k)} = 0$

where $\varphi^{(k)}$ denotes the $k$th-order Eulerian time derivative of $\varphi$.

For illustration, let us present the formulation of $\varphi_{tt}$ in a two-dimensional configuration and for a gravitational potential $\psi = -g\eta$:

$$\varphi_{tt} = \frac{\partial \varphi_t}{\partial t} = \frac{\mathrm{D}_n}{\mathrm{D}t}(\varphi_t) - \frac{\partial \varphi}{\partial n}\frac{\partial \varphi_t}{\partial n} = \frac{\mathrm{D}_n}{\mathrm{D}t}\left[-\frac{1}{2}\left(\frac{\partial \varphi}{\partial n}\right)^2 - \frac{1}{2}\left(\frac{\partial \varphi}{\partial s}\right)^2 + \frac{\sigma}{\rho}\kappa_1 - g\eta\right] - \frac{\partial \varphi}{\partial n}\frac{\partial \varphi_t}{\partial n}.$$

If we refer to Appendices II and III, we can find the necessary tools for the formulation of the advection by the local normal component of velocity.

Finally we obtain

$$\begin{aligned}\varphi_{tt} = &-\frac{\partial \varphi}{\partial n}\frac{\partial \varphi_t}{\partial n} + \left(\frac{\partial \varphi}{\partial n}\right)^2\left(\frac{\partial^2 \varphi}{\partial s^2}\right) - \left(\frac{\partial \varphi}{\partial n}\right)^3 \kappa_1 - \frac{\partial \varphi}{\partial n}\frac{\partial}{\partial s}\left(\frac{\partial \varphi}{\partial n}\right)\frac{\partial \varphi}{\partial s} - \frac{\partial \varphi}{\partial s}\frac{\partial \varphi_t}{\partial s} - \left(\frac{\partial \varphi}{\partial s}\right)^2\frac{\partial \varphi}{\partial n}\kappa_1 \\ &+ \frac{\sigma}{\rho}\frac{\partial^2}{\partial s^2}\left(\frac{\partial \varphi}{\partial n}\right) + \frac{\sigma}{\rho}\frac{\partial \varphi}{\partial n}\kappa_1^2 - g\cos\beta\frac{\partial \varphi}{\partial n}, \end{aligned} \tag{53}$$

the formula which is used for the third-order scheme.

## APPENDIX V: REPRESENTATION OF FIELD FUNCTIONS

To perform the integrations involved in the equations described in Section 2.2, the boundary surface of the computational domain is described by a finite number of discrete points (nodes) and the cubic spline is then used to define the boundary location as a continuous function. For the purpose of integration, interpolation basis functions are then introduced to relate the variation in the primary variables (the unknowns $\Phi$ or $\partial\Phi/\partial n$) within each element to their values at the nodal (extreme) points. We adopt here Hermite polynomial approximation for which the unknowns are located only at the intersection between two elements. Linear interpolating functions ($C^0$ shape basis functions) are mostly used in representing the distribution of the dependent variable over the elements. These shape basis functions are (Figure 12)

$$\Psi(s) = \begin{cases} 0 & \text{if} \quad s \leqslant 1, \\ \omega_2(s-1) & \text{if} \quad 1 < s \leqslant 2, \\ \omega_1(s-2) & \text{if} \quad 2 < s \leqslant 3, \\ 0 & \text{if} \quad s > 3, \end{cases}$$

where

$$\omega_1(s) = 1 - s, \qquad \omega_2(s) = s.$$

In our procedure, to enhance the accuracy of the BEM, we adopt higher-order interpolating functions. The field functions are represented by cubic Hermite polynomial approximations which

 

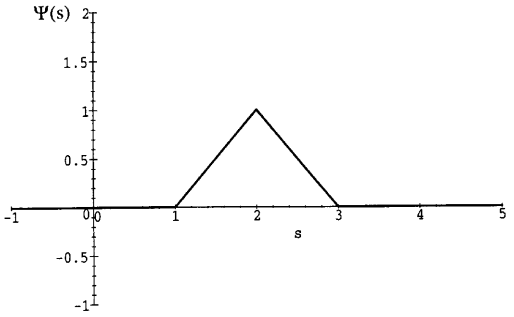


Figure 12. Linear basis function

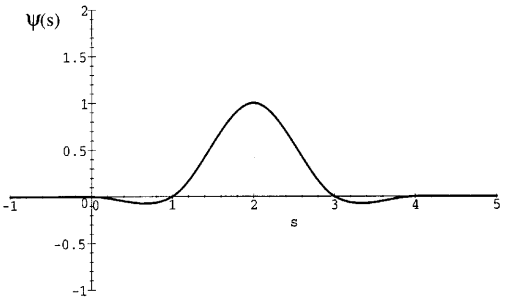


Figure 13. Cubic basis function

has continuous first derivatives between elements. Here the associated $C^1$ basis functions are analytically defined over four elements and have the shape (Figure 13)

$$\Psi(s) = \begin{cases} \frac{1}{2}\omega_4(s) & \text{if} \quad 0 \leqslant s \leqslant 1, \\ \omega_2(s-1) + \frac{1}{2}\omega_3(s-1) & \text{if} \quad 1 < s \leqslant 2, \\ \omega_1(s-2) - \frac{1}{2}\omega_4(s-2) & \text{if} \quad 2 < s \leqslant 3, \\ -\frac{1}{2}\omega_3(s-3) & \text{if} \quad 3 < s \leqslant 4, \end{cases}$$

where

$$\omega_1(s) = (1-s)^2(2s+1), \qquad \omega_2(s) = s^2(3-2s), \qquad \omega_3(s) = s(1-s)^2, \qquad \omega_4(s) = s^2(s-1)$$

and the derivative values are obtained by interpolating three successive points via a parabola. Such basis functions can be viewed as symmetrized Riabenki functions.[21] This allows the accurate calculation of derivative dependent functions (on the boundary) such as velocity. Cubic polynomials can also be used to construct the cubic B-splines which lead to a $C^2$ approximation (continuous first and second derivatives). This latter method has been successfully used by some authors (see e.g. References 14 and 22), but we claim that our approach is simpler and easier to implement.

## REFERENCES

1. M. S. Longuet-Higgins and E. D. Cokelet, 'The deformation of steep surface waves on water. Part I. A numerical method of computation', *Proc. R. Soc. Lond. A*, **350**, 1–26 (1976).
2. J. W. Dold and D. H. Peregrine, 'Steep unsteady water waves: an efficient computational scheme', *Proc. 19th Int. Conf. on Coastal Engineering*, Houston, TX, 1984, pp. 955–967.

 

3. J. W. Dold and D. H. Peregrine, 'An efficient boundary-integral method for steep unsteady water waves', in K. W. Morton and M. J. Baines (eds), *Numerical Methods for Fluid Dynamics II*, Oxford University Press, Oxford, 1986, pp. 671–679.
4. I. Stakgold, *Green's Functions and Boundary Value Problems*, Wiley, 1979.
5. M. A. Jawson and G. T. Symm, *Integral Equation Methods in Potential Theory*, Academic, New York, 1977.
6. M. Abramowitz and I. A. Stegun, *Handbook of Mathematical Functions*, 9th printing, Dover, New York, 1970.
7. C. A. Brebbia, J. C. F. Telles and L. C. Wrobel, *Boundary Element Techniques Theory and Applications in Engineering*, Springer, New York, 1984.
8. L. C. Wrobel, 'Numerical solutions of axisymmetric cavity flows using the boundary element method', *Int. j. numer. methods fluids*, **16**, 845–854 (1993).
9. R. Aris, *Vectors, Tensors and Basic Equations of Fluid Mechanics*, Prentice-Hall, Englewood Cliffs, NJ, 1962.
10. R. M. Bowen and C. C. Wang, *Introduction to Vectors and Tensors, 1. Linear and multilinear Algebra, 2. Vector and Tensor Analysis*, Plenum, New York, 1976.
11. S. T. Grilli, J. Skourup and I. A. Svendsen, 'An efficient boundary element method for nonlinear water waves', *Eng. Anal. Bound. Elem.*, **6**, 97–107 (1989).
12. T. Nakayama, 'A computational method for simulating transient motions of an incompressible inviscid fluid with a free surface', *Int. j. numer. methods fluids*, **10**, 683–695 (1990).
13. A. F. Teles da Silva and D. H. Peregrine, 'Nonlinear perturbations on a free surface induced by a submerged body: a boundary integral approach', *Eng. Anal. Bound. Elem.*, **7**, 214–222 (1990).
14. P. L. F. Liu, H. W. Hsu and M. H. Lean, 'Applications of boundary integral equation methods for two-dimensional non-linear water wave problems', *Int. J. numer. methods fluids*, **15**, 1119–1141 (1992).
15. V. G. Levich, *Physiochemical Hydrodynamics*, Prentice-Hall, Englewood Cliffs, NJ, 1962.
16. J. Vignes, 'A stochastic arithmetic for reliable scientific computation', *Math. Comput. Simul.*, **35**, 233–261 (1993).
17. H. Lamb, *Hydrodynamics*, 6th edn, Cambridge University Press, Cambridge, 1932.
18. C. C. Mei, *The Applied Dynamics of Ocean Surface Waves*, Wiley, New York, 1983.
19. D. G. Dommermuth and D. K. P. Yue, 'Numerical simulations of nonlinear axisymmetric flows with a free surface', *J. Fluid Mech.*, **178**, 195–219 (1987).
20. T. S. Lundgren and N. N. Mansour, 'Oscillations of drops in zero gravity with weak viscous effects', *J. Fluid Mech.*, **194**, 479- -510 (1988).
21. G. Marchouk, *Méthodes de Calcul Numériques*, Mir, Moscow, 1980.
22. J. J. S. P. Cabral, L. C. Wrobel and C. A. Brebbia, 'A BEM formulation using B-splines: I—Uniform blending functions', *Eng. Anal. Bound. Elem.*, **7**, 136–144 (1990).

 